

Fragmentation of a drop as it falls in a lighter miscible fluid

F. T. Arecchi,* P. K. Buah-Bassuah,† F. Francini, and S. Residori
Istituto Nazionale di Ottica, 50125 Firenze, Italy

(Received 25 May 1995; revised manuscript received 20 February 1996)

We report an experimental investigation of the fragmentation process of a heavy drop falling in a lighter miscible fluid. For fixed liquid composition and for different drop sizes, we observe that the fragmentation cascade stops after a few breakups, once each individual droplet has reduced below a critical volume for further splitting. Since each fragmentation is the outcome of a hydrodynamic instability, we expect fluctuations in the size of the fragmented droplets. The main experimental outcomes are the following: (1) the first breakup time scales with the size separation from the critical volume in a universal way independent of the fluid composition; (2) in the region intermediate between the first and the last fragmentation, the droplet sizes display multifractal properties, with the average dimension D_0 decreasing to a minimum and then increasing again once diffusion prevails; and (3) the droplet height scales with time with an exponent independent of the drop volume and composition. [S1063-651X(96)00607-1]

PACS number(s): 47.53.+n, 47.20.-k, 68.10.-m

I. INTRODUCTION

We report the experimental investigation of the transient dynamic phenomena occurring as a liquid droplet falls into a lighter miscible fluid (solvent). The process starts with the deposition of a droplet on the surface of the solvent and terminates by complete mixing. During the transient, there is competition between the breakup induced by the nonlinear hydrodynamic processes and the local damping due to the diffusion of the velocity and concentration [1]. Thus, we observe a transient regime within which the original drop splits into successive families of daughter droplets, with beautiful effects appealing to the aesthetical imagination [2]. A century after the original report [1] the problem has been reconsidered in better detail, showing that the competition between the hydrodynamic instability and diffusional mixing is ruled by two nondimensional numbers, namely, the fragmentation number F [3]

$$F = \frac{g\Delta\rho V}{\mu D} \quad (1)$$

and the Schmidt number S [4]

$$S = \frac{\nu}{D} = \frac{\mu}{\rho D}. \quad (2)$$

In the above relations, g is the gravity acceleration, $\Delta\rho$ is the density difference of the two fluids, ρ is the drop density, V the initial drop volume, μ and ν the dynamic and kinematic viscosities of the solvent, and D the mutual concentration diffusion.

Above a critical value F_c [3], the drop breaks into a number N_1 of fragments which increases as S decreases [4]. If each of the N_1 secondary droplets has an individual fragmentation number still higher than F_c a second breakup occurs.

For the fluid mixtures used in Refs. [3,4], we did not observe fragmentations beyond three steps, since at the third stage the $N=N_1N_2$ tertiary droplets (N_2 =number of fragmentations of each one of the N_1 secondary droplets) were small enough to have an individual fragmentation number below F_c . From this point on, the breakup process stops and mixing continues by pure diffusion. At the end of the breakup process, we are thus faced with a constellation of N droplets of approximately the same size, falling with approximately the same speed, and still connected by thin filaments. We report a sequence of photos showing the morphological details of the fragmentation process (Fig. 1).

The regions occupied by the heavier fluid can be observed

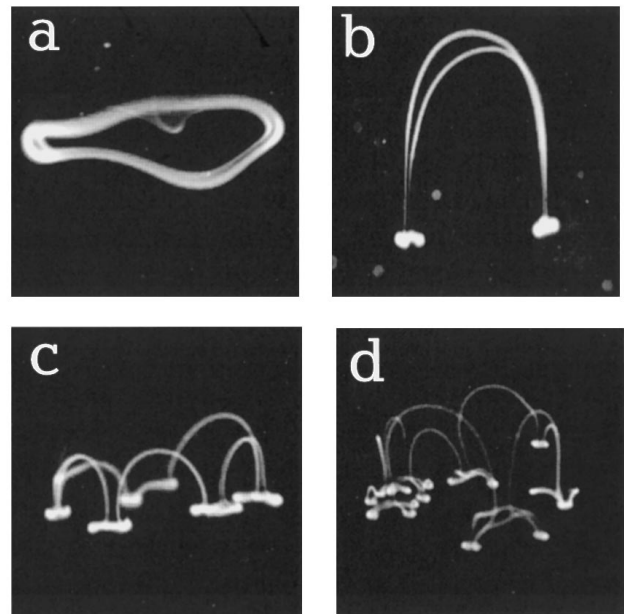


FIG. 1. Side views of a drop falling in a lighter miscible fluid. (a) The drop, initially spherical, has become a torus. Some regions with greater density give rise to successive fragmentations, two in (b) and six in (c). The secondary droplets split again in the last stage of fragmentation (d).

*Also at Physics Dept., University of Florence, Florence, Italy.

†Also at University of Cape Coast, Cape Coast, Ghana.

by doping the initial drop with sodium fluorescein dye in such a small concentration that it would not perturb the hydrodynamic behavior, and yet sufficient to yield a detectable fluorescence under laser illumination. In this way, we can visually detect how the original spherical drop has been spread after breaking up. At an intermediate time, the evolved drop looks like a fractal object embedded in the three-dimensional space provided by the solvent. Projecting such an object, for example, from above onto a screen placed at the bottom of the cell would provide patterns of difficult interpretation, since we are superimposing different sections and hence the same screen region receives contributions from different heights. To solve this problem, we cut a thin horizontal slice by illuminating the cell with a horizontal laser lamina and study the fractal dimension of the set embedded in the two-dimensional slice of illuminated solvent. At any time, we expect to measure a generic multifractal whose average dimension is between 2 and 1, depending on the local trade-off between fragmentation and diffusion.

While the first reports [3,4] were just phenomenological relations between the number of fragments and the two above nondimensional numbers F and S , we present here a detailed experimental investigation. Our main result is that we are able to clearly identify a fragmentation region which is occurring in between the first fragmentation and the onset of a regime dominated by pure diffusion. We are thus faced with three distinct dynamical regions, the first one being mainly ruled by the fragmentation number F , the last one dominated by diffusion, and the intermediate one, in which fragmentation occurs, driven by the hydrodynamic instabilities. The extent of this fragmentation region is determined by the Schmidt number S . We show that this region is characterized by scaling laws with universal exponents, thus we can infer that the fragmentation is a self-similar process. We provide a statistical description of this process by measuring the multifractal structure of the drop concentration distribution.

In Sec. II we present the experimental setup and we report the measurements related to the dynamical behavior of the falling drop. In Sec. III, we report the multifractal structure of the drop concentration distribution, and in Sec. IV we summarize the results.

II. EXPERIMENTAL SETUP AND MEASUREMENTS

A glass cell with a base size of $10 \times 10 \text{ cm}^2$ and 40 cm high, is filled with a solvent of pure distilled water and mounted on a rigid metallic support. On top of the cell is mounted a microsyringe that releases a drop close to the center of the free surface at zero initial velocity and $h=0$ (h being the downward vertical coordinate within the solvent). A collimated Argon laser beam, shaped as a thin lamina by a cylindrical lens, crosses the solvent horizontally. The light lamina has a thickness of approximately $500 \mu\text{m}$ and has a uniform intensity distribution over the whole cell depth. By changing the height of the laminar beam, we can follow the drop at different heights and times.

Beneath the cell is placed a plane mirror, at an angle of 45° , that reflects the fluorescence induced by the passage of the drop through the two-dimensional slice of light. The fragmented drop sections are imaged by an objective onto a

CCD camera consisting of 512 by 512 pixels, then recorded by a VHS video recorder and digitized by a frame grabber with 8-bit resolution. The objective of the camera is adjusted in such a way that the focal depth is sufficiently long to obtain sliced images at different heights through the cell.

Most of the experimental data refer to heavy drops, composed of 15% glycerin and 85% water, seeded with a small amount of sodium fluorescein dye (10^{-5} mol/l). When not otherwise specified, the measurements are carried out for drops with the same concentration ratio but with different volumes. All the reported experiments have been performed under isothermal conditions at a temperature of $20 \pm 0.2^\circ\text{C}$. When we use different drop compositions, we select them from the list of Table I, Ref. 4, where all relevant parameters have been collected.

The fragmentation structure of a liquid drop at different cell heights is ruled by the fluid parameters such as μ , D , ν , ρ , and the cell thickness. We choose a cell size large enough to consider the drop not affected by the lateral cell boundaries.

The experiment was carried out for different drop sizes, corresponding to a drop volume ranging from 2 to $8 \mu\text{l}$ (microlitres). In Fig. 2 we report the recorded horizontal sections of a $4 \mu\text{l}$ drop. The successive images are taken at successive heights. It can be seen [Fig. 2(a)] the initial unperturbed drop and [Figs. 2(b)–2(e)] the beginning of the fragmentation instability with the formation of a torus. Then a first breakup into five fragments takes place [Fig. 2(f)] followed by a further fragmentation of the drop at the second breakup process [Fig. 2(g)]. The last series of images show no further fragmentation but rather the gradual enlargement of the structure until diffusion finally takes over the process [Figs. 2(h)–2(j)].

All the above images were successively recorded from frames with individual pixel intensity greater than the background intensity (above threshold). The square frames ranging from 64×64 up to 320×320 pixels fully contain the region occupied by the drop. The temporal resolution of our measurements is limited by the thickness of the light beam, due to the fact that the drop spends some time in order to cross it. The CCD camera has a standard video acquisition rate, such that each frame lasts 40 ms. Initially, that is at short heights h , the drop takes only one frame time τ to cross the laminar beam. At intermediate and high h the drop takes $n=2$ or 3 frame times to go through the light sheet. A temporal averaging is realized by summing over the n successive frames so that the integration time ranges from 40 to 120 ms.

The successively recorded sections provide an Eulerian description of the process. In order to achieve a link with the Lagrangian point of view, we have to determine the time at which the falling drop reaches a given height. For this purpose, we proceed in the following way. We illuminate a large volume (almost one half) of the entire cell with a white lamp, and then an area of $70 \times 70 \text{ mm}^2$ of the orthogonal side of the cell is imaged on a CCD camera. A graduated scale with millimetric partition is put on the cell and is also imaged. When the drops are released, a video recorder registers on a TV tape the lateral view of the falling drops. The time t of arrival of the drop at a given height h is determined by playing the video tape with a timer. We start the timer when the drop touches the water meniscus and we stop it when the

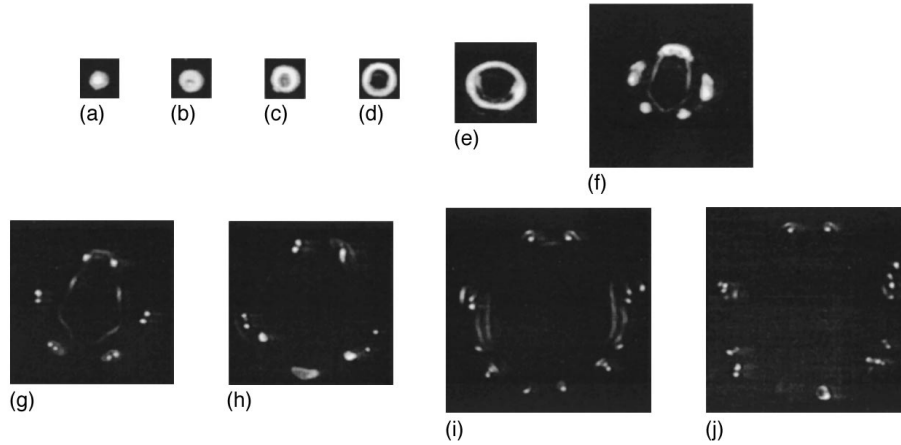


FIG. 2. Horizontal sections of the falling drop at successive heights h : (a) 2.0 mm; (b) 12.0 mm; (c) 17.0 mm; (d) 22.0 mm; (e) 27.0 mm, formation of the torus; (f) 32.0 mm, first breakup with the formation of five fragments; (g) 37.0 mm, second breakup; (h) 42.0 mm; (i) 47.0 mm; and (j) 52.0 mm, enlargement of the fragmented structure. The frame sizes are (a), (b), (c), (d) 64×64 pixels; (e) 128×128 pixels; (f), (g), (h) 256×256 pixels; and (i), (l) 320×320 pixels, and the initial drop volume is $4 \mu\text{l}$.

drop arrives at the selected height, thus obtaining the desired time interval. In order to average the measured time intervals and to reduce the error, we repeat the measurement ten times for each drop volume and each cell height.

The $h(t)$ resulting from the time measurements is reported in Fig. 3 for a drop volume of $2 \mu\text{l}$. From this graph it is evident that there are three distinct regions I–III, each one following a power law $h \sim t^{\gamma_i}$, with different exponents γ_i . The first change (boundary I–II) corresponds to the first breakup whereas the second change (boundary II–III) corresponds to the establishment of pure diffusion. Thus, it can be clearly seen that the intermediate region (II), where fragmentation takes place, is a transient between two distinct situations, that of the whole drop falling down (I) and that of diffusing droplets no more undergoing fragmentations (III).

In Fig. 4 we report the exponents γ_i ($i=I,II,III$), characterizing the three dynamical regions of the falling drop, for

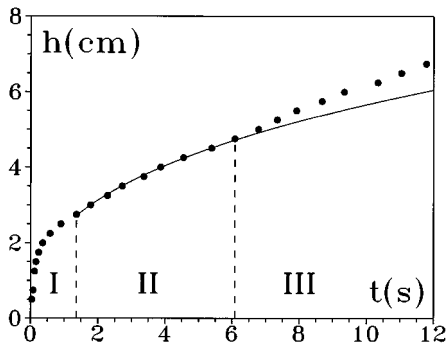


FIG. 3. Measured drop height h as a function of the arrival time t , for an initial drop volume of $2 \mu\text{l}$. The two vertical dashed lines mark, respectively, the occurrence of the first breakup and the onset of pure diffusion without further fragmentations. This way, three regions are identified: (I) that corresponding to the first breakup and ruled mainly by the fragmentation number F , (II) that corresponding to secondary fragmentations and whose extent depends on the Schmidt number S , and (III) that of pure diffusion. The data of region II are fitted with a power law (solid line) whose exponent is about 0.33.

different drop volumes. By fitting the data with a power law, it can be seen that the first exponent γ_I changes with the volume V as $V^{0.50 \pm 0.02}$, the third exponent γ_{III} changes as $V^{0.22 \pm 0.02}$, whereas the second exponent γ_{II} is constant and is 0.34 ± 0.02 . Furthermore, repeating these measurements for different drop compositions, even though, as expected, the sizes of the three regions change, nevertheless the exponent γ_{II} remains the same. Due to the transient character of the phenomenon and to the experimental limitations, the power laws are obtained over a very limited range of data values (less than one decade), nevertheless we think that they can give an interesting suggestion on the universal behavior of the fragmentation process. At least, they are a clear signature of the three distinct dynamical regions which characterize the transient evolution of the fragmentation process.

In particular, this regime is initiated by the first breakup. We can experimentally establish that the breakup time τ_{bu} is the longer, the closer the fragmentation number F is to its

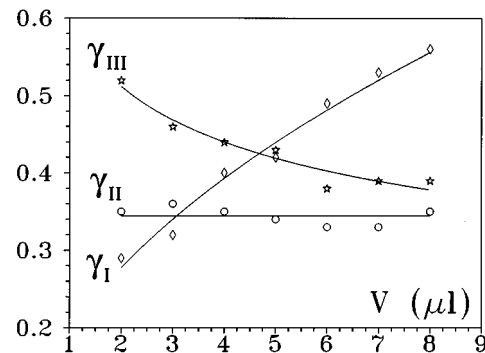


FIG. 4. Scaling exponents γ_I , γ_{II} , and γ_{III} of the height vs time $h \sim t^\gamma$ for the three different regions, respectively, as a function of the initial drop volume V . The points are experimental data and the solid lines are best fits with $\gamma_I \sim V^{0.50 \pm 0.02}$ for the onset of the instability, $\gamma_{III} \sim V^{0.22 \pm 0.02}$ for the onset of diffusion and $\gamma_{II} \sim V^{0.00 \pm 0.02}$ for the fragmentation region. Thus the second region shows a universal behavior with an exponent $\gamma_{II} = 0.34 \pm 0.02$ independent from the initial drop size.

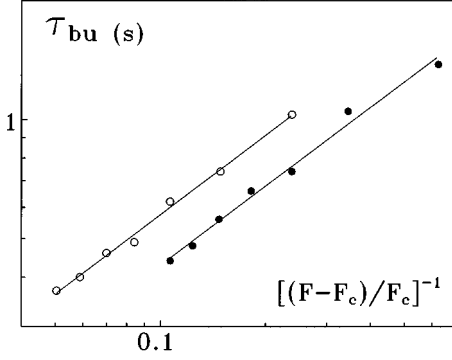


FIG. 5. Breakup time τ_{bu} as a function of the reduced fragmentation number $[(F-F_c)/F_c]^{-1}$ in a log-log plot. Experimental points correspond to two different drop compositions: full dots 15% glycerin and 85% water; empty dots 30% glycerin and 70% water. The best fits (solid lines) give a slope $\beta=0.66\pm 0.05$.

critical value F_c . As said in Ref. [3], it is impossible to disentangle the combined role played by the Kelvin-Helmholtz (KH) and Rayleigh-Taylor (RT) instabilities. However, due to the general character of the phenomenon, we should expect a universal law of the type

$$\tau_{bu} \sim (F - F_c)^{-\beta}, \quad (3)$$

where β is a positive number which does not depend on the fluid composition.

We checked such a conjecture on a series of data. For the fluid composition of Fig. 2 we have $\Delta\rho=3.9\times 10^{-2} \text{ g cm}^{-3}$, $\mu=1\times 10^{-2} \text{ g cm}^{-1} \text{ s}^{-1}$ and $D=9.8\times 10^{-6} \text{ cm}^2 \text{ s}^{-1}$. Thus, the fragmentation number F ranges from 7.3×10^5 to 29.1×10^5 as the drop volume is varied from 2 to 8 μl . The critical fragmentation number F_c is equal to 2.8×10^5 [3]. We report in Fig. 5 the measured breakup times τ_{bu} as a function of the normalized separation from the critical fragmentation number $[(F-F_c)/F_c]^{-1}$ and for two different drop compositions. It can be seen that there is a scaling law as Eq. (3) with an exponent $\beta=0.66\pm 0.05$ which is independent from the drop composition. This result reinforces the indication that the fragmentation process proceed in a universal way, following a quite general scaling law at the onset.

III. TRANSIENT FRACTAL DIMENSION

Images of Fig. 2 are samples of the images chosen for processing. Each digitized image contains levels of the normalized intensity varying from 0 to 255, with a size of the processing box ranging from 64×64 to 320×320 pixels. In order to compute the fractal dimension D_0 of the space occupied by the drop, we adopted a box-counting algorithm [5] consisting in partitioning the space into equally sized cubes of side ε . If $N(\varepsilon)$ is the number of cubes required to cover the space, the Renyi dimension can be calculated according to Eqs. (6)–(8)

$$D_q = \lim_{\varepsilon \rightarrow 0} \frac{1}{q-1} \frac{\ln \sum_{i=1}^{N(\varepsilon)} p_i^q}{\ln(\varepsilon)}, \quad (4)$$

where p_i is the image probability in the i th box defined as follows. In the discrete frame processing, we split the $N\times N$ -pixels frame into $m\times m$ -pixels boxes, where m specifies the (discrete) ε value selected. If we call x (y) the horizontal (vertical) pixel coordinates, then the i th box will span the coordinates from x_i to x_{i+m} and y_i to y_{i+m} . Calling I_{xy} the signal observed at pixel (x,y) , the total signal is given by

$$I_t = \sum_{x,y=1}^N I_{xy}, \quad (5a)$$

whereas the local signal observed in the i th box is given by

$$I_i = \sum_{x=x_i}^{x_{i+m}} \sum_{y=y_i}^{y_{i+m}} I_{xy}. \quad (5b)$$

With this in mind, we define as image probability of the i th box the quantity

$$p_i = \frac{I_i}{I_t}. \quad (5c)$$

Adopting Eq. (4), we calculate the D_q curve for different drops at different heights. The D_q curves are related to the singularity spectrum $f(\alpha)$ by a Legendre transform [8]. The function $f(\alpha)$ describes how densely a singularity of strength α is distributed over the analyzed set. Thus, $f(\alpha)$ can also be seen as the fractal dimension of the subset over which the singularities scale as α and a set characterized by a spectrum of these dimensions is called multifractal since it can be thought of as constituted by many fractal subsets [9,10]. In particular, D_0 , which is the fractal dimension of each image, corresponds to the maximum of $f(\alpha)$ vs α plot.

Figure 6 shows the D_q and the corresponding $f(\alpha)$ curves derived from the analysis of the images recorded at different heights for a drop volume of 4 μl . Due to statistical limitations of our data, D_q are meaningful only in the range $-5 < q < 5$. In Figs. 6(a) and 6(b) we report the results obtained for short heights inside the cell (h from 12 to 47 mm). In this range of heights the fragmentation process takes place, giving rise to a fractalization of the drop set. It can be clearly seen that, starting from a fractal dimension $D_0=2$, this is continuously reducing until it reaches a value close to 1.3. Once the transient fractalization is over, that is, once further fragmentation is inhibited by diffusion, a reverse process, leading to the restoration of the dimension $D_0=2$, takes place as shown in Fig. 6(c), 6(d). This reverse process is rather slow and it can be observed, correspondingly, over a larger range of heights inside the cell (h from 80 to 260 mm). Similar results are obtained for different drop volumes.

The D_0 dimensions extracted from the plots of Fig. 6 are reported, vs the cell height h , in Fig. 7. From this plot it can be seen that up to the onset of the instability (first breakup),

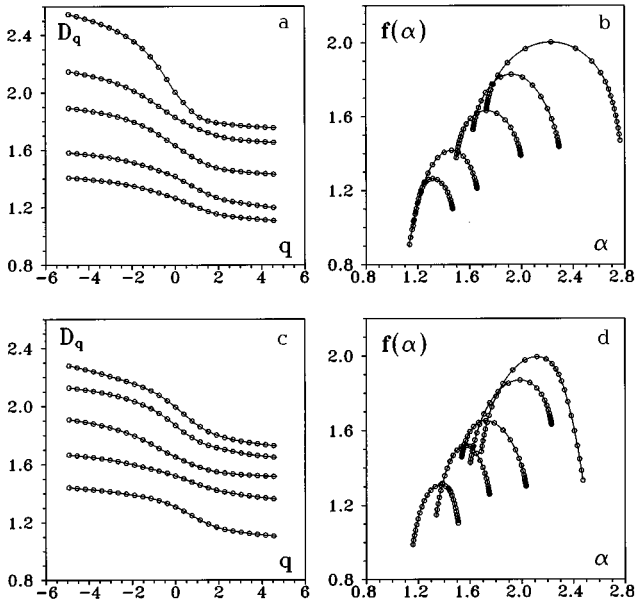


FIG. 6. Multifractal properties of the falling drop. (a), (b) Plots of D_q vs q and of $f(\alpha)$ vs α for different heights ($h=12, 22, 27, 32, 47$ mm from top to bottom). (c), (d) Plots of D_q vs q and of $f(\alpha)$ vs α for different heights ($h=80, 110, 140, 170, 260$ mm from bottom to top). The upper part, (a) and (b), refers to the regime of increasing fractalization (instabilities prevailing over diffusion), the lower part, (c) and (d), to decreasing fractalization (diffusion overcoming instabilities).

D_0 is close to 2. As the fragmentation starts, D_0 decreases gradually down to a value around 1.3. From this point on, diffusion takes over and the transient fractal tends to disappear into a uniform solution of the drop and the solvent, eventually recovering $D_0=2$.

IV. CONCLUSIONS

We have given an experimental characterization of the dynamical and statistical features of a drop falling in a lighter miscible fluid. We have shown that the process can be divided into three distinct dynamical regions, one corresponding to the onset of the first hydrodynamic instability, one characterized by the successive fragmentation of the initial drop into smaller droplets, and one, dominated by diffusion, in which the droplets mix with the solvent without undergoing further fragmentations.

In the fragmentation region the height h reached by the falling drop scales with the corresponding arrival time t as a power law with an exponent $\gamma_{II}=0.34\pm 0.02$ which does not depend on the initial drop volume. Moreover, independently of the fluid composition, the first breakup time scales with the separation from the critical fragmentation number.

The region of fractalization corresponds to a transient process in between the onset of the first instability and pure diffusion. The multifractal structure of the droplet projection at different heights can be interpreted as determined by a distribution of concentration which is related to the self-similar character of the fragmentation process. Therefore, even though we cannot make a direct comparison with similar results obtained for jet turbulence [9], we can infer that

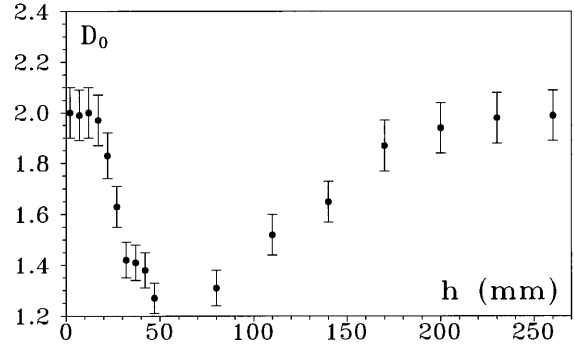


FIG. 7. Measured fractal dimension D_0 as a function of the cell height h , with clear evidence of the two regimes plotted separately in Fig. 6.

the fragmentation cascade has some generic properties of the self-similar processes. In particular, it can be seen as a transient multifractal that could be associated with the breakdown of a single eddy in a turbulent process [11]. On the other hand, we also have the reverse process in the course of which diffusion reestablishes a uniform phase with drop and solvent homogeneously mixed.

From a heuristic point of view, a fragmentation due to hydrodynamic instabilities eventually stopped by diffusion reminds us of the turbulent cascade associated with a high Reynolds number $Re=vr/\nu$. In our case, the F number is the ratio of the diffusion time r^2/D (r being the initial drop radius) to the characteristic time r/v_s ($v_s=g\Delta\rho r^2/\mu$ being the sedimentation velocity) associated with the propagation across the drop radius of hydrodynamic disturbances due to the relative velocity between drop and solvent [3]. Hence, F can be simply written as $F=r v_s/D$ and it looks like a Reynolds number, with the replacement of the kinetic viscosity with the concentration diffusion. Thus our experiment discloses useful analogies with turbulence. As we compare Re and F , while r and v are common to both, replacement of ν with D means going from $10^{-1}-10^{-2}$ cm^2/s to $10^{-5}-10^{-6}$ cm^2/s (see the data of Ref. 6; Table I for μ and D). However, such an analogy which may have a pedagogical value, should not be pushed too far, since the return to a higher dimension here reported is peculiar of a transient regime, whereas turbulent investigations refer to stationary regimes.

In summary, the drop fragmentation is a transient fractal taking place before the establishment of pure mixing between drop and solvent. The extent of this fractal can be controlled by changing the Schmidt number S , which means varying the number of successive fragmentation stages allowed by the trade-off between diffusive and kinematics effects.

ACKNOWLEDGMENTS

P.K.B.-B. acknowledges the International Center for Theoretical Physics (ICTP), Trieste, for financial support under the Associate Scheme and the Office of External Activities, and Istituto Nazionale di Ottica for kind hospitality. We thank P. Bianchi for technical assistance in building the cell. We are grateful to S. Ciliberto for helpful discussions.

- [1] J. J. Thomson and H. F. Newall, Proc. R. Soc. London **39**, 447 (1885).
- [2] D'Arcy W. Thompson, *On Growth and Form*, abridged edition, edited by J. T. Bonner (Cambridge University Press, Cambridge, England 1961).
- [3] F. T. Arecchi, P. K. Buah-Bassuah, F. Francini, C. Perez-Garcia, and F. Quercioli, Europhys. Lett. **9**, 333 (1989).
- [4] F. T. Arecchi, P. K. Buah-Bassuah, and C. Perez-Garcia, Europhys. Lett. **15**, 429 (1991).
- [5] H. Froehling, J. P. Crutchfield, D. Farmer, N. H. Packard, and R. Shaw, Physica D **3**, 605 (1981).
- [6] P. Grassberger and I. Procaccia, Physica D **3**, 34 (1984).
- [7] P. Grassberger, Phys. Lett. **107A**, 101 (1985).
- [8] T. C. Hasley, M. H. Jensen, L. P. Kadanoff, I. Procaccia, and B. I. Shraiman, Phys. Rev. A **33**, 1141 (1986).
- [9] R. R. Prasad, C. Meneveau, and K. R. Sreenivasan, Phys. Rev. Lett. **61**, 76 (1988).
- [10] J. Feder, *Fractals* (Plenum, New York, 1988).
- [11] H. Tennekes and J. L. Lumley, *A First Course in Turbulence* (MIT, Cambridge, MA, 1972).